The Johns Hopkins University

IN-32
80330
32 p.

ELECTRICAL ENGINEERING & COMPUTER SCIENCE

Interim Progress Report on NAG-356

"Optical Communication with Semiconductor Laser Diodes"

F. Davidson

This report covers the period Jan. 1 - June 30, 1987 and takes the form of the paper "Gaussian Approximation versus Nearly Exact Performance Analysis of Intersatellite Optical Communication Links with PPM Signaling and Low Noise APD Receivers" which has been submitted for journal publication.

Gaussian Approximation versus Nearly Exact Performance Analysis of Intersatellite Optical Communication Links With PPM Signaling and Low Noise APD Receivers*

F. M. Davidson and X. Sun

Department of Electrical and Computer Engineering
The Johns Hopkins University
Baltimore, MD 21218

ABSTRACT

A 25 megabit/second direct detection optical communication system that used Q=4 PPM signaling was constructed and its performance measured under laboratory conditions. The system used a single mode AlGaAs laser diode transmitter and low noise silicon avalanche photodiode (APD) photodetector. Comparison of the measured performance of the system with that was theoretically expected revealed that modeling the APD output as a Gaussian process under conditions of negligible background radiation and low (less than 10^{-12}A) APD bulk leakage currents leads to substantial underestimates of optimal APD gain to use and overestimates of system bit error probability. A procedure is given to numerically compute system performance which uses the more accurate Webb's Approximation of the exact Conradi distribution for the APD output signal that does not require excessive amounts of computer time (a few minutes of VAX 8600 CPU time per system operating point). Examples are given which illustrate the breakdown of the Gaussian approximation in assessing system performance. This system achieved a bit error probability of 10^{-6} at a received signal energy corresponding to an average of 60 absorbed photons/bit and optimal APD gain of 700. The measured performance of the system was found to be in excellent agreement with the performance predicted by the nearly exact computational procedure used.

* Work supported by the National Aeronautics and Space Administration

I Introduction

Recent advances in the technology of both semiconductor laser diodes [1]-[4] and low noise silicon avalanche photodetectors (APDs) [5]-[7] have generated considerable interest in free-space direct detection optical communication between satellites. Theoretical analyses of optical communication systems (both free-space and fiber-optic guide) that contain an APD as a photodetector have appeared previously [8]-[10]. Due to the complicated nature of the statistical description of the response of the APD to incident photons, nearly all these analyses have modeled the APD output as a Gaussian process. The actual distribution of secondary electrons output by the APD in response to the absorption of primary photons has been given by McIntyre and Conradi [11] [12]. Use of the Gaussian approximation in the calculation of system bit error probabilities has been shown to be quite accurate in situations where the bulk leakage current of the APD itself is of order of nanoamperes, the APD gain is a few hundred, and background light levels are not negligible [13],[14]. In systems that use on-off keying as the modulation format, the optimal receiver consists of a threshold test [15]. In this instance, modeling the APD output as a mixture random variable consisting of the discrete number of APD output photoelectrons and continuous Gaussian thermal noise as an equivalent Gaussian random variable has been theoretically shown to be quite accurate, provided certain conditions are met [16].

The modulation format of choice in semiconductor laser diode direct detection optical links consists of low order PPM signaling [17]. The optimal receiver [15] consists of a device which determines the time slot which contained the largest APD output signal; no comparisons against fixed thresholds are required. Furthermore, silicon APD's with bulk leakage currents below 1.0 picoampere and values of k_{eff} (ratio of the ionization coefficients of holes and electrons) of less than 0.01 are now readily available commercially [18]. These devices are conventional silicon APD structures and do not require fabrication of superlattice devices in which $k_{eff}=0$.

A theoretical analysis of the measured performance characteristics of a AlGaAs laser diode direct detection optical communication system that contained a low noise APD photodetector will be described here. It shows that use of the

Gaussian approximation for the APD output can lead to substantial underestimates of optimal APD gain and substantial overestimates of receiver error probabilities under conditions of very low background light levels likely to be encountered in satellite-to-satellite or deep space optical communication links. The reason for the discrepancy is that the Gaussian approximation does not accurately describe the low noise APD output signal in time slots that contain only low level background light. In addition, an efficient numerical computation procedure will be given for calculating receiver error probabilities that does not involve use of the Gaussian approximation. This procedure is shown to be in good agreement with measured system bit error rates.

The remainder of this paper is organized as follows. The next section gives the details of the nearly exact numerical computation procedure for the determination of bit error probabilities that does not require excessive amounts of computer time. It is shown that as the number of background light counts per time slot is decreased, use of the Gaussian approximation causes larger and larger discrepancies in predicted values of optimal APD gain and system bit error probabilities. The last section describes the prototype laser diode optical communication system which was operated at a source data rate of 25 megabits/second, used Q=4 PPM signaling and achieved a bit error probability of 10^{-6} at a received signal energy corresponding to, on average, 60 absorbed photons per information bit (120 photons/PPM symbol). The theoretically computed performance is shown to be in good agreement with the experimentally measured performance. The nearly exact procedure for calculating system performance correctly predicts not only the optimal APD gain (which can be found experimentally), but actual system error probabilities as well.

II Theoretical Analysis

The probability that n photons are absorbed from an incident optical field of known intensity, $P_o(t)$ watts, by a photoelectric effect detector over an interval [t,t+T] is given by a Poisson distribution of mean $\bar{n}=\frac{\eta}{hf}\int_t^{t+T} P_o(t')dt'$, where η is the quantum efficiency with which the detector converts incident photons to

photoelectrons, and hf is the incident photon energy. In the case of APD photodetectors, primary photoelectron-hole pairs undergo an avalanche multiplication process which results in the output of m electrons from the APD in response to the absorption of, on average, $\overline{n}$ primary photons. The integer random variable m cannot be less than the number of absorbed photons and is characterized by the Conradi distribution [12]

$$P(m \mid \overline{n}) = \sum_{n=1}^{\infty} \frac{n\Gamma(\frac{m}{1-k_{eff}}+1)}{m(m-n)!\,\Gamma(\frac{k_{eff}m}{1-k_{eff}}+1+n)} [\frac{1+k_{eff}(G-1)}{G}]^{\frac{n+k_{eff}m}{1-k_{eff}}} \tag{1}$$

$$\cdot [\frac{(1-k_{eff})(G-1)}{G}]^{m-n} \cdot \frac{(\overline{n})^n}{n!} e^{-\overline{n}}, \qquad m \geq 1$$

where G is the average APD gain. Due to the randomness of the gain mechanism in the APD, the output signal is characterized by an excess noise factor defined as $F = E\{m^2\}/E^2\{m\}$, which can be shown to be [12]

$$F = k_{eff}G + (2-1/G)(1-k_{eff}) \tag{2}$$

Silicon APDs have quantum efficiencies of nearly 80% at wavelengths around 800 nm, and values of k_{eff} as low as 0.006 [7]. In addition, all APD's have both bulk and surface leakage currents which are nonzero. This results in nonzero output current in the total absence of incident photons. Currently available low noise silicon APD's have surface leakage currents of about 10 nanoamperes, and bulk leakage currents of 1.0 picoamperes or less [18].

In Q-ary PPM signaling, L binary source bits are transmitted as a single light pulse in one of $Q = 2^L$ possible time slots once every T seconds. The output waveform has constant average power and peak power Q times larger. Semiconductor laser diodes are both peak and average power limited. As long as Q is not so large as to cause facet damage in the laser, PPM signaling produces high peak power short duration pulses that become more easily distinguished from background and thermal noise as Q is increased. Peak power limitations of the semiconductor laser generally limit Q to values of 8 or less [17] [19].

The optimal receiver for this communication format consists of a device which integrates the APD output signal over each time slot and then chooses the largest as the slot that contained the received light pulse. Figure 1 shows a block diagram of the system. The PPM word error probability (WEP) can be written as [9]

$$WEP = 1 - \int_{-\infty}^{\infty} p(x \mid \lambda_1 T_s) \left[\int_{-\infty}^{x} p(x' \mid \lambda_0 T_s) dx' \right]^{Q-1} dx \tag{3}$$

and the corresponding bit error probability (BEP) as

$$BEP = \frac{Q}{2(Q-1)} WEP \tag{4}$$

$p(x \mid \lambda T_s)$ is the probability density function for the integrated output from each time slot. λ_1 represents the photon absorption rate due to received signal and background radiation and λ_0 is the photon absorption rate due to background radiation alone. T_s is the slot time period.

The electrical charge integrated over each time slot is defined as x. Conditioned on the number of secondary photoelectrons, $p(x \mid \lambda T_s)$ can be written as

$$p(x \mid \lambda T_s) = \sum_{m=0}^{\infty} p(x \mid m) P(m \mid \lambda T_s) \tag{5}$$

The accumulated charge during each slot consists of the APD output electrons and any additive amplifier thermal noise charge. Given the secondary electrons, m, x is a Gaussian random variable with probability density

$$p(x \mid m) = \phi(x, \bar{x}_m, \sigma^2) \equiv \frac{1}{\sqrt{2\pi\sigma}} e^{-\frac{(x-\bar{x}_m)^2}{2\sigma^2}} \tag{6a}$$

$$\bar{x}_m = me + I_s T_s \tag{6b}$$

$$\sigma^2 = (2eI_s + \frac{4KT}{R}) BT_s^2 \tag{6c}$$

In equation (6), e = electron charge, K = Boltzmann's constant, T = equivalent noise temperature, I_s = APD surface leakage current, and B = one sided noise bandwidth. The APD surface leakage current, I_s, dose not get multiplied by the APD gain and therefore can be treated as a constant DC current. The APD bulk leakage current does get multiplied by the APD gain and can be modeled as part

of the background radiation.

$P(m \mid \lambda T_s)$, given by (1) with $\bar{n} = \lambda T_s$, has been approximated with good accuracy by Webb [20] as

$$P(m \mid \lambda T_s) = \frac{1}{(2\pi\lambda T_s G^2 F)^{1/2}} \cdot \frac{1}{[1+\frac{m-G\lambda T_s}{\lambda T_s GF/(F-1)}]^{3/2}} \cdot \exp\left[- \frac{(m-G\lambda T_s)^2}{2\lambda T_s G^2 F(1+\frac{m-G\lambda T_s}{G\lambda T_s F/(F-1)})}\right] \tag{7}$$

for m values greater than λT_s. Equation (7) approaches a Gaussian density with mean $G\lambda T_s$ and variance $FG^2\lambda T_s$ for values of m close to its mean, i.e., $|(m-G\lambda T_s)| << G\lambda T_s$. Figure 2 plots (7) and its corresponding Gaussian approximation, for λT_s equal to unity and 120 respectively. As can be seen, the true distribution of secondary electrons skews toward the right and departs greatly from a Gaussian at both tails. These are the regions which form the main contribution to the PPM word error probability. It is also noticed that at very small mean number of primary incident photons, e.g. $\lambda T_s=1$, The Gaussian shape is not even close to the shape of the true distribution. Even worse, the Gaussian extends into the region of negative numbers of secondary electrons, which is clearly unphysical. Nevertheless, due to its simplicity, the Gaussian model is widely used in evaluating error probabilities of optical communication systems.

If the distribution of secondary electrons, m, is assumed Gaussian, the charge accumulated during each time slot, which is the sum of secondary electrons and amplifier thermal noise, is also a Gaussian random variable. Therefore,

$$P(x \mid \lambda T_s) = \frac{1}{\sqrt{2\pi\sigma}} e^{-\frac{(x-\mu)^2}{2\sigma^2}} \tag{8a}$$

$$\mu = eG\lambda T_s + I_s T_s \tag{8b}$$

$$\sigma^2 = (2e^2G^2F\lambda + 2eI_s + \frac{4KT}{R}) BT_s^2$$

$$= e^2G^2F\lambda T_s + eI_s T_s + \frac{2KTT_s}{R} \tag{8c}$$

where λ is given by $\lambda_s+\lambda_b+I_b/e$ or λ_b+I_b/e. λ_b represents the photon absorption rate due to the actual background light and I_b/e represents the contribution of the APD bulk leakage current to the APD output. Here B is taken to be $1/2T_s$ and is the equivalent noise bandwidth of an ideal integrator. The power spectral density of the shot noise from the APD is taken to be $d<i^2>/df = 2e^2\lambda G^2F$ as given by Smith and Personick [8].

It was found during the course of our experiments that at low background radiation levels, for example, $(\lambda_b+I_b/e)T_s \approx 0.01$, the use of the Gaussian approximation significantly underestimated the optimal average APD gain and overestimated the error probabilities. That can be understood as follows. In the extreme situation when $(\lambda_b+I_b/e)T_s=0$, the APD output from time slots where no light pulse was transmitted consists of only the amplifier thermal noise which is independent of APD gain. The error probability can then be reduced by increasing the APD gain, because the distribution of the output from those slots that do contain light pulses will be shifted and skewed to the right, away from the distribution of the output from slots that contain no light pulse. That implies an optimal APD gain of infinity and an optimal error probability which is infinitesimal. On the other hand, when the Gaussian approximation is used, increasing the APD gain not only shifts the distribution but also spreads it out symmetrically rather than skews it towards the right. The probability that the APD output is smaller than a fixed threshold x_0 is

$$P(x \leq x_0) = \int_{-\infty}^{x_0} \frac{1}{(2\pi e^2 G^2 F \lambda_s T_s)^{1/2}} \exp\left[\frac{-(x-eG\lambda_s T_s)^2}{2e^2G^2F\lambda_s T_s}\right]dx \qquad (9a)$$

$$= \int_{-\infty}^{T} \frac{1}{\sqrt{2\pi}} e^{-\frac{t^2}{2}} dt$$

where

$$T = \frac{x_0 - eG\lambda_s T_s}{(e^2G^2F\lambda_s T_s)^{1/2}} \qquad (9b)$$

Here the amplifier noise has been ignored. It can be seen that $T \to 0$ as $G \to \infty$ for any value of x_0 because F is proportional to G, and consequently $P(x \leq x_0) \to 1/2$ as $G \to \infty$. That is to say that the optimal APD gain cannot be

infinite and the minimal error probability never reduces to the infinitesimal. In reality, $\lambda_b>0$ and $I_b>0$ but as long as $(\lambda_b+I_b/e)T_s$ is small, the Gaussian approximation still underestimates the optimal gain and overestimates the error probabilities. The smaller $(\lambda_b+I_b/e)T_s$ gets, the bigger the discrepancies become.

Very low noise APDs have bulk leakage currents of less than 10^{-12} amperes [18], which is equivalent to a background radiation count rate of order 10^6/second. Background light levels in space are negligible unless the sun or the earth enters the field of view of the receiver optics [21]. At useful data transmission rates of 100 megabits/second and higher, the mean number of background counts per slot, $(\lambda_b+I_b/e)T_s$, can be well below unity. The Gaussian approximation does not accurately model the APD output under these conditions. Consequently, a more accurate approximation to the Conradi distribution for the APD output must be used to correctly predict the system performance for very low background noise levels.

Substituting (5) and (6) into (3), the PPM word error probability can be written as

$$WEP = \sum_{m=0}^{\infty} P(m \mid \lambda_1 T_s) \int_{-\infty}^{\infty} \phi(x,\bar{x}_m,\sigma^2) \cdot\{ 1-[\sum_{m'=0}^{\infty} P(m' \mid \lambda_0 T_s) Erf(\frac{x-\bar{x}_{m'}}{\sigma})]^{Q-1}\} dx \tag{10}$$

where

$$Erf(u) \equiv \int_{-\infty}^{u} \phi(x,0,1)dx = \int_{-\infty}^{u} \frac{1}{\sqrt{2\pi}} e^{-\frac{t^2}{2}} dt \tag{11}$$

$\bar{x}_m$ and $\bar{x}_{m'}$ are the mean values of charge x for given secondary electrons m and m′ respectively. Since $Erf(\frac{x-\bar{x}_{m'}}{\sigma}) = 1-Erf(-\frac{x-\bar{x}_{m'}}{\sigma})$, $\bar{x}_{m'} \ll \bar{x}_m$, and x varies about its mean during the course of the outer integration in (10), $Erf(-\frac{x-\bar{x}_{m'}}{\sigma}) \ll 1$. We can then use a Talor expansion for the Q-1 power and approximate the expression inside the braces of (10) and rewrite WEP as

$$\text{WEP} = (Q-1)\sum_{m=0}^{\infty} P(m \mid \lambda_1 T_s)\int_{-\infty}^{\infty} \phi(x,\bar{x}_{m,}\sigma^2)$$

$$\cdot \sum_{m'=0}^{\infty} P(m' \mid \lambda_0 T_s)\text{Erf}(-\frac{x-\bar{x}_{m'}}{\sigma})dx \qquad (12)$$

This is equivalent to the union bound for the word error probability.

In a numerical evaluation of (12), the two infinite sums and the infinite integral have to be truncated to finite terms and limits. Equation (12) can be rewritten as

$$\text{WEP} = (Q-1)\sum_{m=0}^{M} P(m \mid \lambda_1 T_s)\int_{A_m}^{B_m} \phi(x,\bar{x}_{m,}\sigma^2)$$

$$\cdot \sum_{m'=0}^{M'} P(m' \mid \lambda_0 T_s)\text{Erf}(-\frac{x-\bar{x}_{m'}}{\sigma})dx$$

$$+ (Q-1)\sum_{m=M+1}^{\infty} P(m \mid \lambda_1 T_s)\int_{-\infty}^{\infty} \phi(x,\bar{x}_{m,}\sigma^2)$$

$$\cdot \sum_{m'=0}^{\infty} P(m' \mid \lambda_0 T_s)\text{Erf}(-\frac{x-\bar{x}_{m'}}{\sigma})dx$$

$$+ (Q-1)\sum_{m=0}^{M} P(m \mid \lambda_1 T_s) \int_{x<A_m,\, x>B_m} \phi(x,\bar{x}_{m,}\sigma^2)$$

$$\cdot \sum_{m'=0}^{\infty} P(m' \mid \lambda_0 T_s)\text{Erf}(-\frac{x-\bar{x}_{m'}}{\sigma})dx$$

$$+ (Q-1)\sum_{m=0}^{M} P(m \mid \lambda_1 T_s)\int_{A_m}^{B_m} \phi(x,\bar{x}_{m,}\sigma^2)$$

$$\cdot \sum_{m'=M'+1}^{\infty} P(m' \mid \lambda_0 T_s)\text{Erf}(-\frac{x-\bar{x}_{m'}}{\sigma})dx$$

$$\approx (Q-1)\sum_{m=0}^{M} P(m \mid \lambda_1 T_s)\int_{A_m}^{B_m} \phi(x,\bar{x}_{m,}\sigma^2)$$

$$\cdot \sum_{m'=0}^{M'} P(m' \mid \lambda_0 T_s)\text{Erf}(-\frac{x-\bar{x}_{m'}}{\sigma})dx \qquad (13)$$

The resultant error consists of three parts corresponding to each truncation. A

set of bounds for those errors are given in Appendix, along with the procedure for choosing the appropriate limits of the sums and the integral. The procedure to evaluate equation (13) is as follows. First, the limits of the integral for a fixed value of the index of the outer sum, m, A_m and B_m, are computed. Corresponding to each value of the integration variable, x, the inner sum and then the integrand are evaluated. The integration is multiplied by $P(m \mid \lambda_1 T_s)$ and the product is then accumulated. The process repeats for all values of m from zero to M. The subroutines for the integration and error function Erf(u) in (13) were called from the IMSL library.

The use of Webb's approximation, (7), for $P(m \mid \lambda T_s)$ in (13) rather than the exact Conradi distribution given by (1) greatly reduces the computational time needed to evaluate the WEP. However, Webb's approximation is only valid for $m > \lambda T_s > 0$ and terms corresponding to $m \leq \lambda_1 T_s$ and $m' \leq \lambda_0 T_s$ have to be treated separately. The contributions from the terms for $m \leq \lambda_1 T_s$ in the outer sum of (13) are negligible since $P(m \mid \lambda_1 T_s) \rightarrow 0$ for values of m which are much less than its mean, $G\lambda_1 T_s$. On the other hand, the contributions from the terms for $m' = 0$ in the inner sum of (13) cannot be neglected when $\lambda_0 T_s \ll 1$. The probability that no secondary electrons are output by the APD, $P(m' = 0 \mid \lambda_0 T_s)$, is given by $e^{-\lambda_0 T_s}$, the same as the probability that no primary electron is generated based on the Poisson distribution. If both $\lambda_b T_s$ and $I_b T_s/e$ approach zero, which occurs at high data rates , low background radiation level, and low APD bulk leakage current, the probability that no secondary electron is output by the APD approaches unity. In other words, when $\lambda_0 T_s \ll 1$, the contribution of the term for $m' = 0$ in (13) must be taken into account and equation (13) should be modified as

$$\begin{aligned} WEP \approx (Q-1) \sum_{m=\lambda_1 T_s}^{M} P(m \mid \lambda_1 T_s) \int_{A_m}^{B_m} \phi(x, \bar{x}_{m,} \sigma^2) \\ \cdot \sum_{m'=1}^{M'} P(m' \mid \lambda_0 T_s) Erf\left(-\frac{x-\bar{x}_{m'}}{\sigma} \right) dx \\ + (Q-1) \sum_{m=\lambda_1 T_s}^{M} P(m \mid \lambda_1 T_s) \cdot e^{-\lambda_0 T_s} \cdot \int_{A_m}^{B_m} \phi(x, \bar{x}_{m,} \sigma^2) Erf\left(-\frac{x-I_s T_s}{\sigma} \right) dx \end{aligned} \qquad (14)$$

where I_sT_s is the value of $\bar{x}_{m'}$ at $m' = 0$. $P(m \mid \lambda_1 T_s)$ and $P(m' \mid \lambda_0 T_s)$ are given by Webb's approximation, (7). The contribution from the second term in (14) increases as $\lambda_0 T_s$ decreases. In the extreme case when $\lambda_0 T_s = 0$, the second term in (14) becomes the only contribution to WEP and the first term vanishes because

$$\sum_{m=\lambda_1 T_s}^{M} P(m \mid \lambda_1 T_s) \int_{A_m}^{B_m} \phi(x, \bar{x}_m, \sigma^2) \sum_{m'=1}^{M'} P(m' \mid \lambda_0 T_s) \mathrm{Erf}\left(-\frac{x - \bar{x}_{m'}}{\sigma}\right) dx$$

$$\leq \sum_{m'=1}^{\infty} P(m' \mid \lambda_0 T_s)$$

$$= 1 - e^{-\lambda_0 T_s} \rightarrow 0, \quad \text{as } \lambda_0 T_s \rightarrow 0$$

Even more computation time can be saved by increasing the summation indices in (14) by increments bigger than unity with subsequent multiplication of individual terms by the value of the increments. Special care must be taken for small values of m' where $P(m' \mid \lambda_0 T_s)$ changes rapidly as m' increases. Experience showed that m' should be incremented by unity over the range $1 \leq m' < 100$. Trial and error methods indicated that differences in the results from trial to trial could be maintained below 1% for increments of m and m' (when $m' \geq 100$) which were of the order of several hundred.

III Experiments and Measurements

A prototype optical communication system was constructed with the use of of a GaAlAs laser diode (Sharp LT024MD) as the transmitter and a low noise APD (RCA C30902S) as the photodetector. The system used Q=4 PPM signaling and operated with a source data rate of 25 megabits per second. A detailed description of the system is given in [22]. The integrations shown in Figure 1 were realized with the use of a matched filter which had a tapped delay line structure described in [22]. Both the PPM modulator and demodulator shared the same timing signal (i.e. the same slot clock) for the sake of simplicity. A timing recovery system must be provided at the receiver in an actual system.

The bit error probabilities of the system were measured as follows. A pseudorandom binary sequence 1023 bits long was input to the PPM modulator. The recovered binary bit stream from the PPM demodulator was then directly compared with the properly delayed version of the transmitted binary sequence with the use of an exclusive OR gate. The gate output was sampled at the source bit rate to avoid miscounting burst errors. A counter then read out the average error frequency. The bit error probability was computed by dividing the average error frequency by the bit rate. The counter recored at least 100 error events before an average error frequency was computed.

The average optical power received by the APD was measured by removing the APD and substituting the sensor of an optical power meter which had a much larger active area than that of the APD. No other changes were made to the optics during the measurements. The APD was then repositioned and the average error frequency was again determined. The data were abandoned if the two average error frequencies had changed by more than 10%. This was done to avoid the effects of any drift in optical power during the course of the measurements. The average number of signal photons contained in each PPM word, which is the same as the average number of photons contained in each laser pulse if $\lambda_0 \ll \lambda_1$, was determined through the relation

$$\lambda_1 T_s = \frac{\eta Q P_{av} T_s}{hf} \tag{15}$$

where P_{av} is the average incident optical power in watts registered by the optical power meter and the quantum efficiency, η, was taken to be 77%. There are $L=\log_2 Q$ source bits in each PPM word and consequently the average number of photons for each bit is $\lambda_1 T_s/\log_2 Q$.

The optimal average APD gain for a fixed input optical power level was determined by adjusting the APD reverse bias voltage until the error probability reached a minimum. The actual value of the APD gain was measured as follows. The APD preamplifier output signal was displayed on an oscilloscope, and the average value of the peak height of the output in time slots that contained the received light pulse was estimated by inspection. Since the conversion factor, g (transimpedance amplifier gain in volts/amperes), of the APD preamplifier was

known, the average APD gain is given by

$$G = \frac{V/g}{e\eta Q P_{av}/hf} \tag{16}$$

where V is the average peak amplitude of the APD response in volts.

Amplifier noise can be neglected compared with the APD excess noise if a strong cw optical field illuminates the APD. The excess noise factor, F, can then be determined by measuring the noise power output by the preamplifier over a known bandwidth. The noise power spectral density is given by [13].

$$\frac{d}{df}\langle i^2\rangle = 2e^2 \frac{\eta P_{cw}}{hf} G^2 F \tag{17}$$

Here P_{cw} is the incident optical power measured with an optical power meter and $d\langle i^2\rangle/df$ is determined by dividing the noise power by the bandwidth over which the noise power was measured. This method assumed the noise output was white, which was confirmed by direct measurement of the power spectrum of the APD output signal over the range dc to 100 MHz under conditions of constant intensity illumination. The excess noise factor F was computed from (17), and (2) was then used to compute k_{eff}. Measurements made at several values of APD gain gave values of k_{eff} of 0.010.

The APD load resistor was 1030 Ω as given by the manufacturer of the preamplifier and its effective noise temperature was found to be approximately 1100 °K. This result was obtained by measuring the noise power output of the preamplifier when the APD bias voltage was reduced to nearly zero (i.e. $G \approx 0$) so that only amplifier thermal noise was present.

Equation (17) was also used to determine the background radiation levels through the relation

$$\lambda_0 = \lambda_b + \frac{I_b}{e} = \frac{1}{2e^2 G^2 F} \frac{d}{df}\langle i^2\rangle_b \tag{18}$$

Here $\langle i^2\rangle_b$ represents the part of the noise power density contributed by the actual background radiation and the bulk leakage current of the APD. It is found as the difference between the total measured noise power density and the contribution from the preamplifier determined previously. However, (18) could not be

used to determine accurately the equivalent background noise count rate due to the bulk leakage current of the low noise APD, I_b/e, by eliminating all the real background light ($\lambda_b=0$), because the noise at the APD output due to the APD bulk leakage current was only a few percent of the amplifier noise. However, I_b/e could be calculated from the data supplied by the manufacturer of the APD for the spectral noise density in dark, i.e. $(d<i^2>/df)^{1/2} = 3\times10^{-13}A/Hz^{1/2}$ at G=600 [18]. I_b/e is then given by the right hand side of (18) which was 0.0122 per PPM slot time (20ns) corresponding to $I_b=9.79\times10^{-14}A$. The APD surface leakage current is found by using the relationship

$$I_d = GI_b + I_s \tag{19}$$

where I_d is the total APD dark current. For the APD used, I_d was 12×10^{-9} A as stated by the manufacturer, the APD surface leakage current was then $11.9\times10^{-9}A$, about the same as the total dark current. The noise density due to this surface leakage current at the front end of the preamplifier was $(2eI_s)^{1/2}=6.2\times10^{-14}A/Hz^{1/2}$, and the noise density due to the APD load resistor of 1030 Ω at the equivalent noise temperature 1100°K was $(4KT/R)^{1/2}=7.3\times10^{-12}$, much larger than that due to the surface leakage current. Therefore the APD surface leakage current had little effect on the measurements and system performance.

Figure 3 shows the results of numerical evaluations of the bit error probability as a function of the average APD gain based on equation (14) for the optical inputs indicated in the graph. The curve with $\lambda_0T_s=12.5$ corresponds to $I_b=0.1nA$ if $\lambda_b=0$, and the curve with $\lambda_0T_s=0.0122$ corresponds to our actual experimental conditions where no real background light was present. The results based on the Gaussian approximation are also plotted (dashed curve) for the purpose of comparison. The measured optimal APD gain with $\lambda_0T_s=0.0122$ was 700, which was in good agreement with the numerically computed results based on (14) as shown in Figure 3. The Gaussian approximation works well for $\lambda_sT_s=12.5$ but very poorly for $\lambda_0T_s=0.0122$. The validity of equation (14) was further tested experimentally under the condition $\lambda_0T_s=1$, which was set by arbitrarily introducing background light according to (17). The measured optimal APD gain was 580, close to what the numerical evaluation had predicted, as

shown in Figure 4.

Figures 5 through 7 are the numerical results of bit error probabilities as a function of the average number of photons required to transmit one bit of information, i.e. $\bar{n}_s/\text{bit} \equiv \lambda_1 T_s/\log_2 Q$, under $\lambda_0 T_s=12.5$, $\lambda_0 T_s=1$, and $\lambda_0 T_s=0.0122$ respectively. Figure 5, once again, shows the appropriateness of Gaussian approximation under $\lambda_0 T_s=12.5$. The small crosses in Figure 6 and Figure 7 are the experimental results under each background noise level, and they are all very close to the numerical computation results based on equation (14). These results substantiate the validity of the numerical evaluation procedure described in the previous section. The Gaussian approximation is accurate only for high levels of background noise level and gets worse and worse as the average number of background noise counts decreases. At $\lambda_0 T_s=0.0122$ and $\lambda_1 T_s=110$, use of the Gaussian model underestimated the optimal APD gain by almost a factor of two and overestimated the bit error probability by more than two orders of magnitude over what was actually measured in the experiments.

In the numerical computations, the subroutine for the integration in (14) was set to have a relative error less than 1%. The limits of the two sums in (14), M and M' , were chosen according to the procedure given in Appendix. As an example, at $\lambda_1 T_s=110$, $\lambda_0 T_s=0.0122$ and G=700, $M \approx 119{,}000$ and $M' \approx 133{,}000$, the proper increments for the indices m and m' (when $m' \geq 100$) of the sums in (14) were 2,200 and 500 respectively. Therefore about 50 points were taken to estimate the outer sum and about 350 points (including 100 points for $0 \leq m' \leq 99$) were taken to estimate the inner sum. As a result, the CPU time required to compute one value of WEP was about two minutes on a VAX 8600 computer.

Appendix

Limits of the Summations and Integration in (13)

From Eq.(13), the truncation error is

$$e = e_1 + e_2 + e_3 \tag{A1.a}$$

$$e_1 \equiv (Q-1) \sum_{m=M+1}^{\infty} P(m \mid \lambda_1 T_s) \tag{A1.b}$$

$$\cdot \int_{-\infty}^{\infty} \phi(x,\bar{x}_m,\sigma^2) \sum_{m'=0}^{\infty} P(m' \mid \lambda_0 T_s) \mathrm{Erf}(-\frac{x-\bar{x}_{m'}}{\sigma})dx$$

$$e_2 \equiv (Q-1) \sum_{m=0}^{M} P(m \mid \lambda_1 T_s) \tag{A1.c}$$

$$\cdot \int_{x>B_m,\ x<A_m} \phi(x,\bar{x}_m,\sigma^2) \sum_{m'=0}^{\infty} P(m' \mid \lambda_0 T_s) \mathrm{Erf}(-\frac{x-\bar{x}_{m'}}{\sigma})dx$$

$$e_3 \equiv (Q-1) \sum_{m=0}^{M} P(m \mid \lambda_1 T_s) \int_{A_m}^{B_m} \phi(x,\bar{x}_m,\sigma^2) \tag{A1.d}$$

$$\cdot \sum_{m'=M'+1}^{\infty} P(m' \mid \lambda_0 T_s) \mathrm{Erf}(-\frac{x-\bar{x}_{m'}}{\sigma})dx$$

where M and M′ are the upper limits of the sums, and A_m and B_m are the lower and upper limits of the integral. Since probabilities do not exceed unity and $\mathrm{Erf}(-\frac{x-\bar{x}_{m'}}{\sigma}) \leq 1$ for any value of x,

$$e_2 < (Q-1) \sum_{m=0}^{M} P(m \mid \lambda_1 T_s) \cdot \int_{x>B_m,\ x<A_m} \phi(x,\bar{x}_m,\sigma^2)dx \tag{A2.a}$$

The integrand in (A2.a) is now a Gaussian density function and A_m and B_m can be chosen such that the integration is a constant for any value of m. Then,

$$e_2 < (Q-1) \int_{x>B_m,\ x<A_m} \phi(x,\bar{x}_m,\sigma^2)dx \tag{A2.b}$$

A_m and B_m can be set to be symmetric about $\bar{x}_m$ and deviate by an amount which is determined by the specified maximum value for e_2. For example, $A_m = \bar{x}_m - 6\sigma$ and $B_m = \bar{x}_m + 6\sigma$ for $e_2 < (Q-1) \times 10^{-9}$.

Next, since $\bar{x}$ and $\bar{x}_{m'}$ become further apart as m increases, the value of the integration in (A1.b) decreases monotonically as m increases. Therefore,

$$e_1 < (Q-1) \sum_{m=M+1}^{\infty} P(m \mid \lambda_1 T_s)$$

$$\cdot \int_{-\infty}^{\infty} \phi(x,\bar{x}_{M+1},\sigma^2) \sum_{m'=0}^{\infty} P(m' \mid \lambda_0 T_s) \cdot \mathrm{Erf}(-\frac{x-\bar{x}_{m'}}{\sigma})dx$$

$$< (Q-1) \int_{-\infty}^{\infty} \phi(x,\bar{x}_{M+1},\sigma^2) \sum_{m'=0}^{\infty} P(m' \mid \lambda_0 T_s) \cdot \mathrm{Erf}(-\frac{x-\bar{x}_{m'}}{\sigma})dx$$

$$\approx (Q-1) \int_{A_{M+1}}^{B_{M+1}} \phi(x,\bar{x}_{M+1},\sigma^2) \sum_{m'=0}^{M'} P(m' \mid \lambda_0 T_s) \cdot \mathrm{Erf}(-\frac{x-\bar{x}_{m'}}{\sigma})dx \qquad (A3)$$

Hence it is safe to choose M such that the integral given in (A3) is less than a specified value (e.g. 10^{-9}). The integral in (A3) is identical to that in (13) when taking m=M+1, so proper values of M can be determined during the course of the numerical evaluation of (13), rather than through trials of separate computations of (A3). Every time the index of the outer sum is increased, i.e. a new term is computed and accumulated for the outer sum of (13), the values of the integral within this new term is compared with a preset limit, for example, $10^{-9}/(Q-1)$ for $e_1 < 10^{-9}$. The process terminates when the value of the integral in the next new term becomes less than the preset limit.

Finding the proper value of M′ is lengthy. First, since $\mathrm{Erf}(-\frac{x-\bar{x}_{m'}}{\sigma}) \leq 1$ for any value of x,

$$e_3 \leq (Q-1) \sum_{m=0}^{M} P(m \mid \lambda_1 T_s) \int_{A_m}^{B_m} \phi(x,\bar{x}_m,\sigma^2)dx \cdot \sum_{m'=M'+1}^{\infty} P(m' \mid \lambda_0 T_s)$$

$$< (Q-1) \sum_{m'=M'+1}^{\infty} P(m' \mid \lambda_0 T_s). \qquad (A4.a)$$

Substituting (7) for $P(m' \mid \lambda_0 T_s)$ in (A4.a) and then bounding the sum by the associated integral gives,

$$e_3 < (Q-1)\int_{M'}^{\infty} \frac{1}{(2\pi\lambda_0 T_s G^2 F)^{1/2}} \cdot \frac{1}{[1+\frac{m' - G\lambda_0 T_s}{\lambda_0 T_s GF/(F-1)}]^{3/2}} \qquad \text{(A4.b)}$$

$$\cdot \exp\left[- \frac{(m' - G\lambda_0 T_s)^2}{2\lambda_0 T_s G^2 F(1+\frac{m' - G\lambda_0 T_s}{G\lambda_0 T_s F/(F-1)})}\right] dm'$$

Since, for $m' > G\lambda_0 T_s$

$$(1+\frac{m' - G\lambda_0 T_s}{G\lambda_0 T_s F/(F-1)}) < (1+\frac{m' - G\lambda_0 T_s}{G\lambda_0 T_s}) = \frac{m'}{G\lambda_0 T_s}$$

then,

$$2\lambda_0 T_s G^2 F(1+\frac{m' - G\lambda_0 T_s}{G\lambda_0 T_s F/(F-1)}) < 2GFm' \ .$$

The exponent in (A4.b) satisfies

$$\frac{(m' - G\lambda_0 T_s)^2}{2\lambda_0 T_s G^2 F(1+\frac{m' - G\lambda_0 T_s}{G\lambda_0 T_s F/(F-1)})} > \frac{(m' - G\lambda_0 T_s)^2}{2GFm'}$$

$$> \frac{m'^2 - m' G\lambda_0 T_s}{2GFm'}$$

$$= \frac{m' - G\lambda_0 T_s}{2GF}.$$

Also

$$[1 + \frac{m' - G\lambda_0 T_s}{\lambda_0 T_s GF/(F-1)}]^{3/2} > [\frac{m' - G\lambda_0 T_s}{\lambda_0 T_s GF/(F-1)}]^{3/2},$$

then,

$$e_3 < \frac{Q-1}{(2\pi\lambda_0 T_s G^2 F)^{1/2}} \int_{M'}^{\infty} \frac{1}{[\frac{m' - G\lambda_0 T_s}{\lambda_0 T_s GF/(F-1)}]^{3/2}} \qquad \text{(A4.c)}$$

$$\cdot \exp\left[-\frac{m' - 2\lambda_0 T_s G}{2GF}\right] dm'$$

Let $u \equiv \frac{2GF}{m' - \lambda_0 T_s G}$, so that

$$e_3 < \frac{1}{2}(Q-1)\lambda_0 T_s e^{\lambda_0 T_s/2F} \cdot \sqrt{\frac{F}{\pi(F-1)^3}} \cdot \int_0^{\frac{2GF}{M' - \lambda_0 T_s G}} \frac{1}{\sqrt{u}} e^{-\frac{1}{u}} du \qquad \text{(A4.d)}$$

The proper value of M' is found by setting the upper limit of the integral in (A4.d) such that e_3 is smaller than a desired value. Following are two examples with two sets of the parameters used in the experiments described in section III.

Example 1:

$\lambda_0 T_s = 1$, $k_{eff} = 0.01$, $G = 500$, $Q = 4$. For $e_3 < 10^{-9}$,

$$\frac{2GF}{M' - \lambda_0 T_s G} < 0.067, \quad \text{or } M' > 105{,}000$$

Example 2:

$\lambda_0 T_s = 0.01$, $k_{eff} = 0.01$, $G = 700$, $Q = 4$. For $e_3 < 10^{-9}$,

$$\frac{2GF}{M' - \lambda_0 T_s G} < 0.095, \quad \text{or } M' > 133{,}000$$

References

[1] J. D. Barry, "Design and system requirements imposed by the selection of GaAs/GaAlAs single mode laser diodes for free space optical communications," *IEEE J. Quantum Electronics*, vol. QE-20, pp. 478-491, May 1984.

[2] J. P. Van der Ziel, H. Temkin, R. A. Logan and R. Dupuis, "High-power picosecond pulse generation in GaAs multiquantum well phase-locked laser arrays using pulsed current injection," *IEEE J. Quantum Electronics*, vol. QE-20, pp. 1236-1242, Nov. 1984.

[3] D. R. Scifres, R. P. Burnham and W. Streifer, "High power coupled multiple stripe quantum well injection lasers," *Applied Physics Letters*, vol. 41, pp. 118-120, July 1982.

[4] J. Katz, S. Margalit and A Yariv, "Diffraction coupled phase locked semiconductor laser array," *Applied Physics Letters*, vol. 42, pp. 554-556, April 1983.

[5] P. P. Webb and R. J. McIntyre, "Recent developments in silicon avalanche photodiodes," *RCA Engineering*, vol 27, pp. 96-102, 1982.

[6] M. C. Teich, K. Matsuo and B. E. A. Saleh, "Excess noise factors for conventional and superlattice avalanche photodiodes and photomultiplier tubes," *IEEE J. Quantum Electronics*, vol. QE-22, pp. 1184-1193, Aug. 1986.

[7] M. C. Teich, K. Matsuo and B. E. A. Saleh, "Counting distributions and error probabilities for optical receivers incorporating superlattice avalanche photodiodes," *IEEE Trans. Electron Devices*, vol. ED-33, pp.1475-1488, Oct. 1986.

[8] R. G. Smith and S. D. Personick, "Receiver design for optical fiber communication systems," in *Semiconductor Devices for Optical Communication*, ch. 4, New York: Spring-Verlag, 1980.

[9] J. B. Abshire, "Performance of OOK and low-order PPM modulations in optical communications when using APD-based receivers," *IEEE Trans. Commun.*, vol. COM-32, no. 10, pp. 1140-1143, Oct. 1984.

[10] N. Sorensen and R. Gagliardi, "Performance of optical receivers with avalanche photodetection," *IEEE Trans. Commun.*, vol. COM-27, pp. 1315-1321, Sept. 1979.

[11] R. J. McIntyre, "The distribution of gains in uniformly multiplying avalanche photodiodes: Theory," *IEEE Trans. Electron Devices*, vol. ED-19, pp. 703-713, June 1972.

[12] J. Conradi, "The distribution of gains in uniformly multiplying avalanche photodiodes: Experimental," *IEEE Trans. Electron Devices,* vol. ED-19, pp. 713-718, June 1972.

[13] S. D. Personick, P. Balaban and J. H. Bobsin, "A detailed comparison of four approaches to the calculation of the sensitivity of optical fiber system receivers," *IEEE Trans. Commun.*, vol. COM-25, no. 5, pp. 211-221, May 1977.

[14] L. L. Jeromin and V. W. S. Chan, "Performance of a coded optical communication system using an APD direct detection receiver," *IEEE International Conference of Communications (ICC'83)*, Boston, MA, June 19-22, 1983,

Conf. Proc., pp. 235-244.

[15] D. L. Snyder, *Random Point Processes*, ch. 2, New York: John Wiley and sons, Inc., 1975.

[16] R. M. Gagliardi and G. Prati, "On Gaussian error probabilities in optical receivers," *IEEE Trans. Commun.*, vol. COM-28, pp. 1742-1747, Sept. 1980.

[17] J. Katz, "Average power constraints in AlGaAs semiconductor lasers under pulse-position-modulation conditions," *Optics Communications*, vol. 56, pp. 330-333, Jan. 1986.

[18] RCA data sheet on C30902E, C30902S, C30921E, C30921S avalanche photodiodes.

[19] G. S. Mecherle, "Impact of laser diode performance on data rate capability of PPM optical communication," *IEEE Military Communications Conference (MilCom'85),* Boston, MA, Oct. 20-23, 1985, Conf. Proc., vol. 1, pp. 115-121.

[20] P. P. Webb, "Properties of avalanche photodiodes," *RCA Review*, vol. 35, pp. 234-278, June 1974.

[21] L. Frecon, and E. Sein, "Optical intersatellite data link with semiconductor laser," *International Astronautical Federation, Intern'l Astronautical Congress, 35 th*, Lausanne, Switzerland, Oct. 7-13, 1984, IAF paper, pp. 84-69.

[22] X. Sun and F. Davidson, "Performance measurements of a diode laser optical communications link with Q=4 PPM signaling," *SPIE Meeting*, Jan. 12-16, 1986, Los Angles, CA, Conference 756.

Figure Captions

Fig. 1. Block diagram of an optimal PPM receiver.

Fig. 2. Distribution of number of secondary electrons, m, output by an APD, given $\lambda T_s \equiv$ the average number of absorbed photons. The solid curves are calculated using (7) and the dashed curves correspond to the Gaussian density function with mean $= G\lambda T_s$ and variance $= G^2F\lambda T_s$.

Fig. 3. Probability of bit error vs. average APD gain. The solid curves are calculated using (14) and the dashed curves are based on the Gaussian approximation. Other parameter values used were: APD load resistor R=1030Ω, equivalent noise temperature T=1100 °K, APD surface leakage current I_s=11.9nA and PPM slot period $T_s = 20$ ns.

Fig. 4. Same as Fig. 3, but at a different background radiation level.

Fig. 5. Probability of bit error vs. average number of photons required to transmit one bit of information. The solid curves are calculated using (14) and the dashed curves are based on the Gaussian approximation. Other parameters were the same as in Fig. 3.

Fig. 6. Same as Fig. 5, but at a different background radiation level. The Gaussian approximation used G=450, the optimal value according to Fig. 3. The crosses represent the experimentally measured data.

Fig. 7. Same as Fig. 5, but at a different background radiation level. The Gaussian approximation used G=450, the optimal value according to Fig. 4. The crosses represent the experimentally measured data.

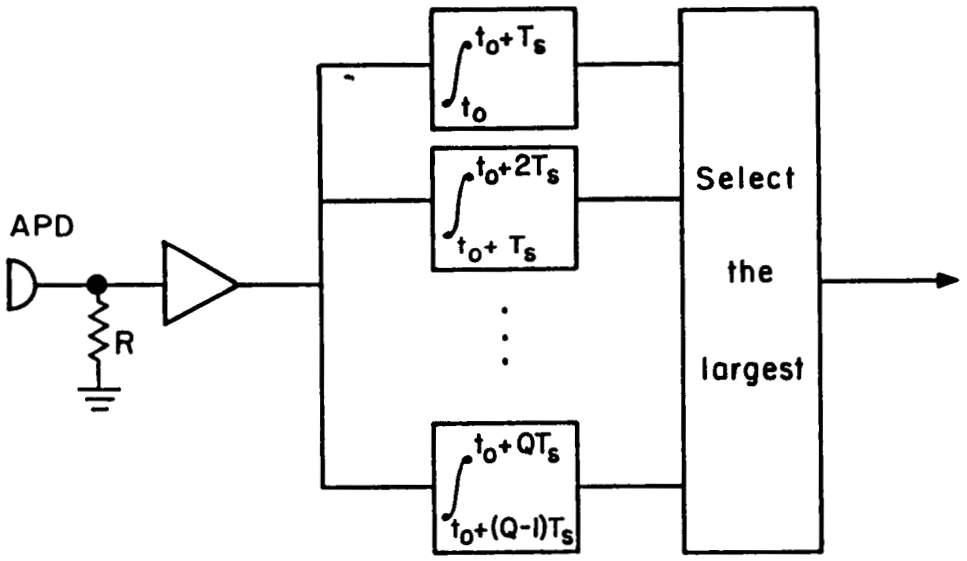
APD
R
$\int_{t_0}^{t_0+T_s}$
$\int_{t_0+T_s}^{t_0+2T_s}$
$\int_{t_0+(Q-1)T_s}^{t_0+QT_s}$
Select
the
largest

Figure 1

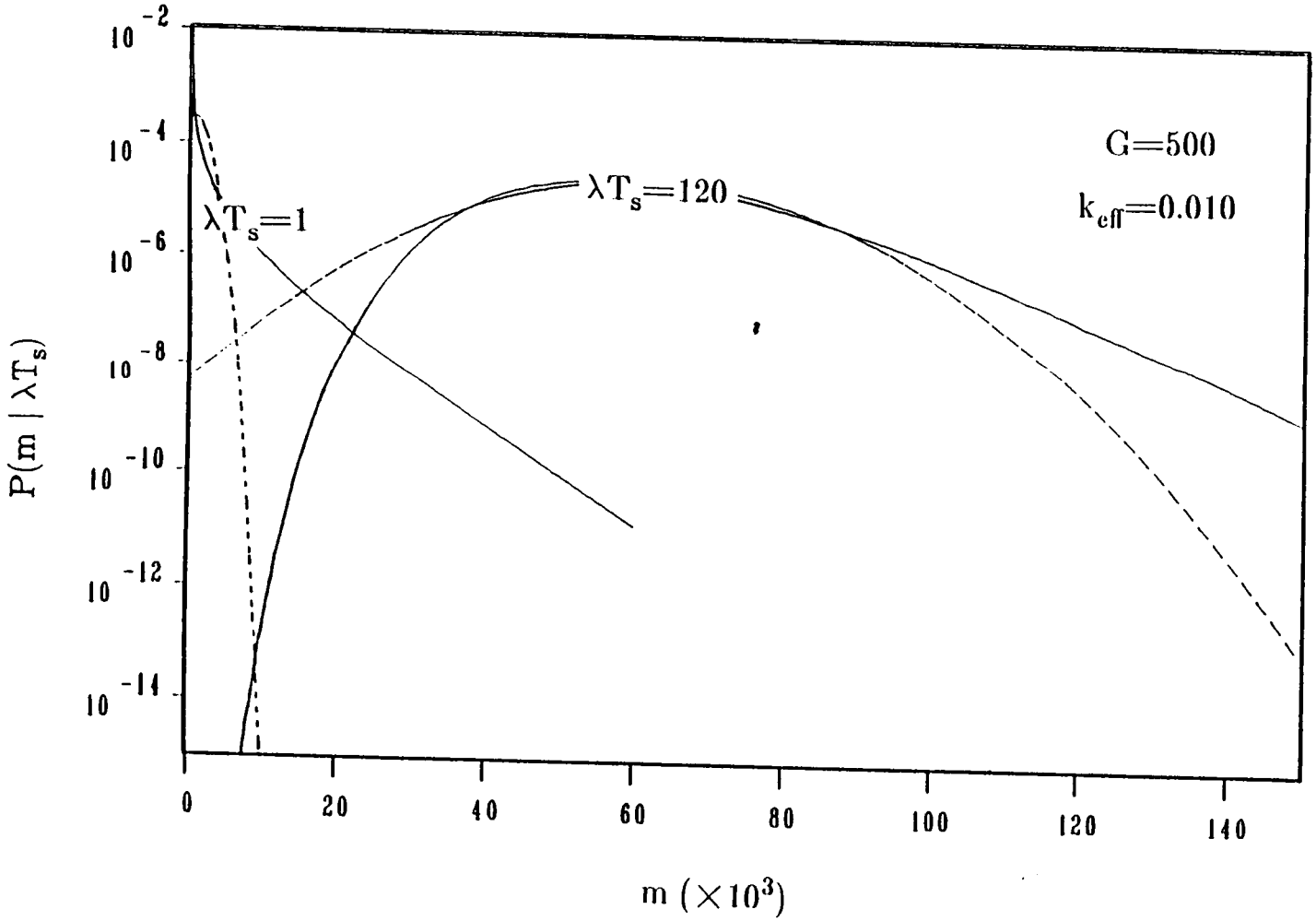
10^{-2}
10^{-4}
10^{-6}
10^{-8}
10^{-10}
10^{-12}
10^{-14}
$P(m \mid \lambda T_s)$
$\lambda T_s=1$
$\lambda T_s=120$
G=500
$k_{eff}=0.010$
0
20
40
60
80
100
120
140
m ($\times 10^3$)

Figure 2

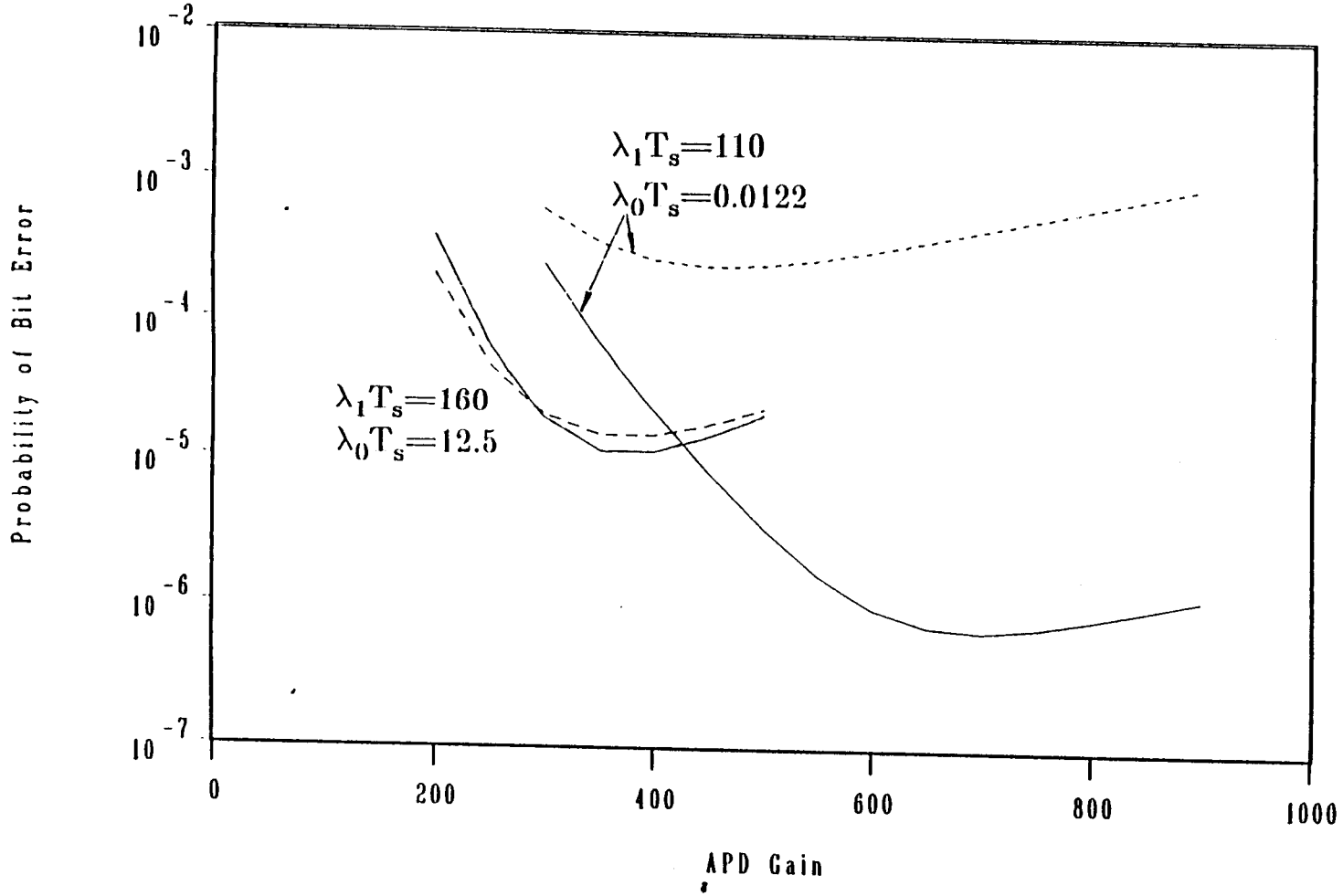
Probability of Bit Error
10^{-2}
10^{-3}
10^{-4}
10^{-5}
10^{-6}
10^{-7}
$\lambda_1 T_s = 110$
$\lambda_0 T_s = 0.0122$
$\lambda_1 T_s = 160$
$\lambda_0 T_s = 12.5$
0
200
400
600
800
1000
APD Gain

Figure 3

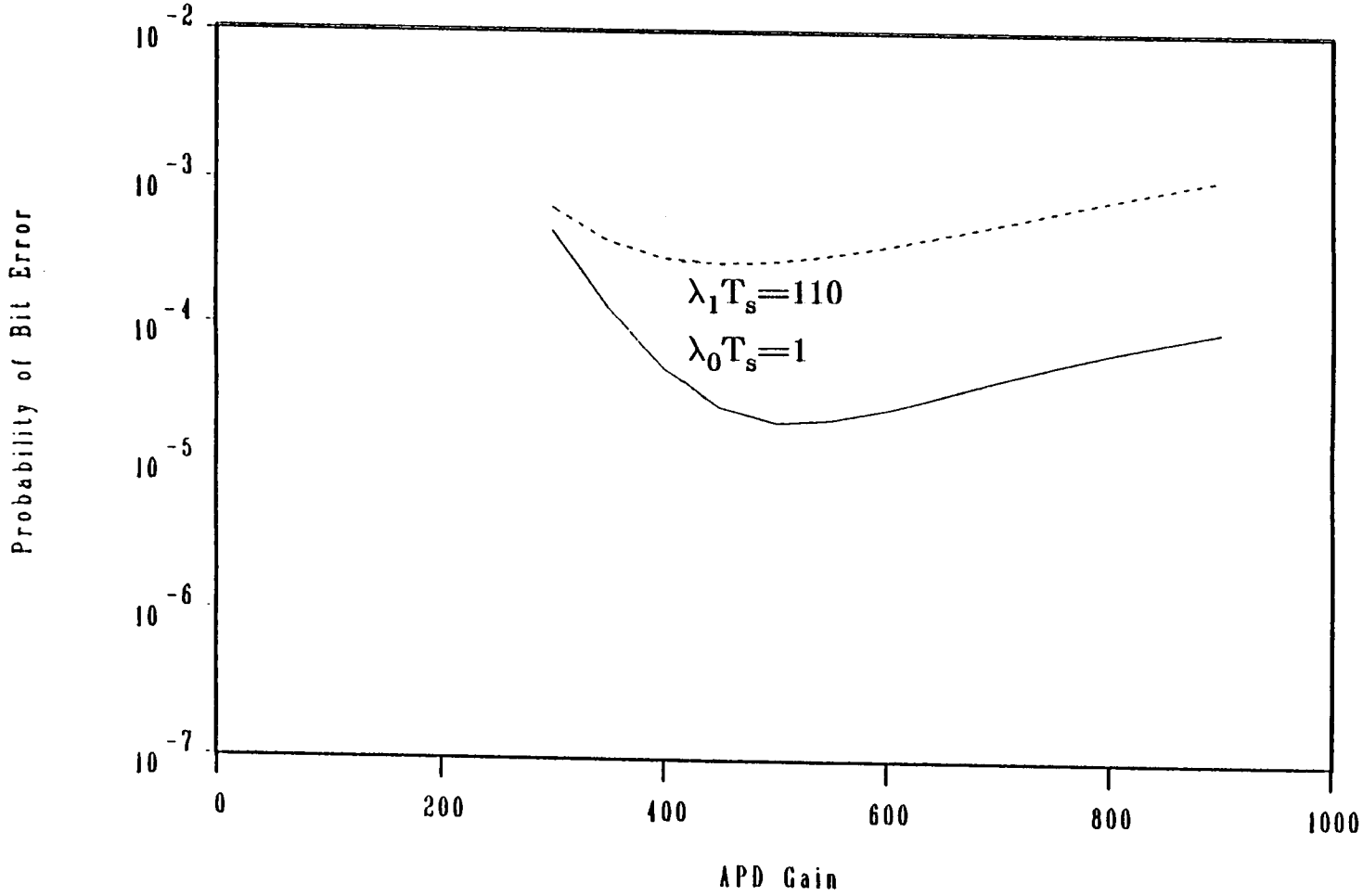
Probability of Bit Error
10^-2
10^-3
10^-4
10^-5
10^-6
10^-7
λ1Ts=110
λ0Ts=1
0
200
400
600
800
1000
APD Gain

Figure 4

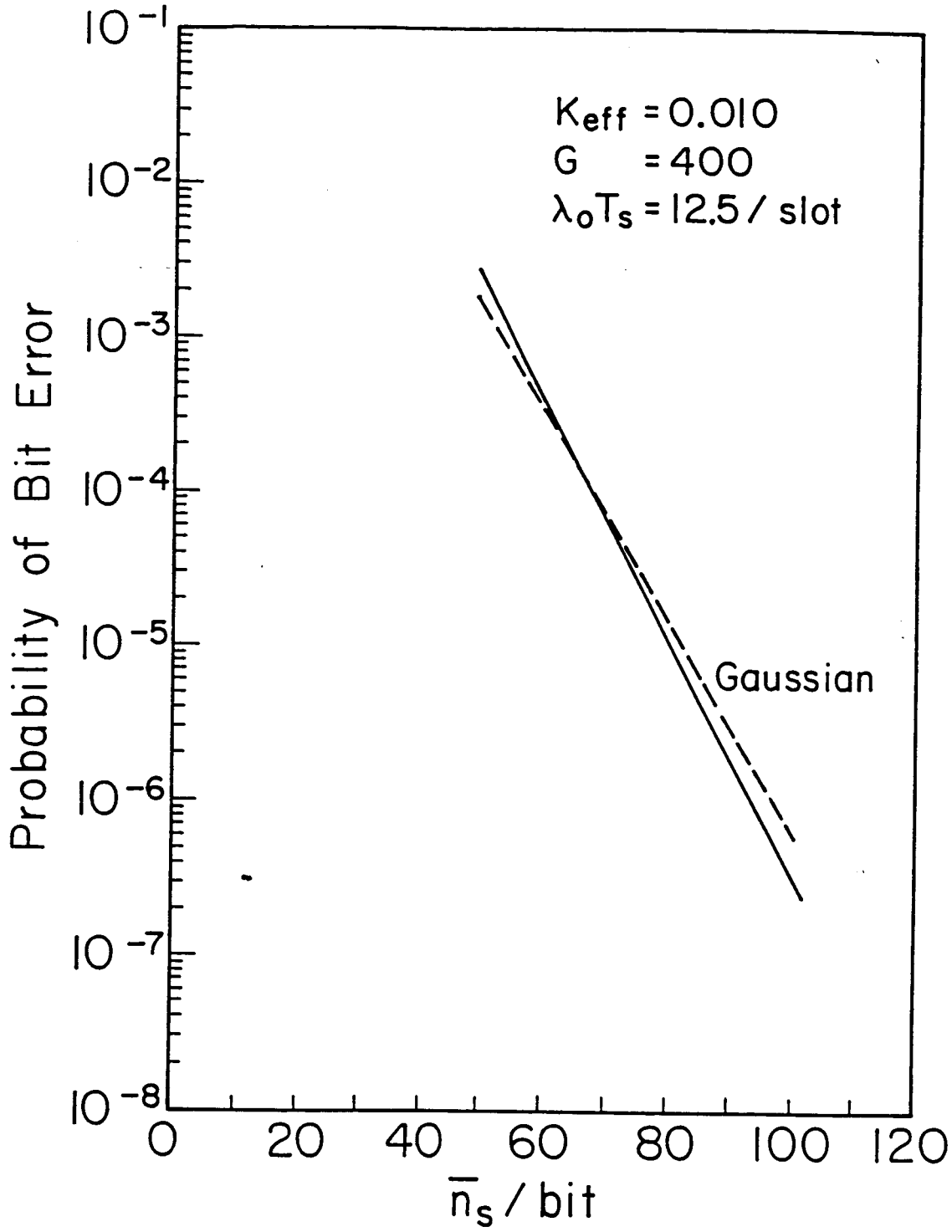
10^{-1}
10^{-2}
10^{-3}
10^{-4}
10^{-5}
10^{-6}
10^{-7}
10^{-8}
Probability of Bit Error
K_{eff} = 0.010
G = 400
$\lambda_o T_s$ = 12.5 / slot
Gaussian
0
20
40
60
80
100
120
$\bar{n}_s$ / bit

Figure 5

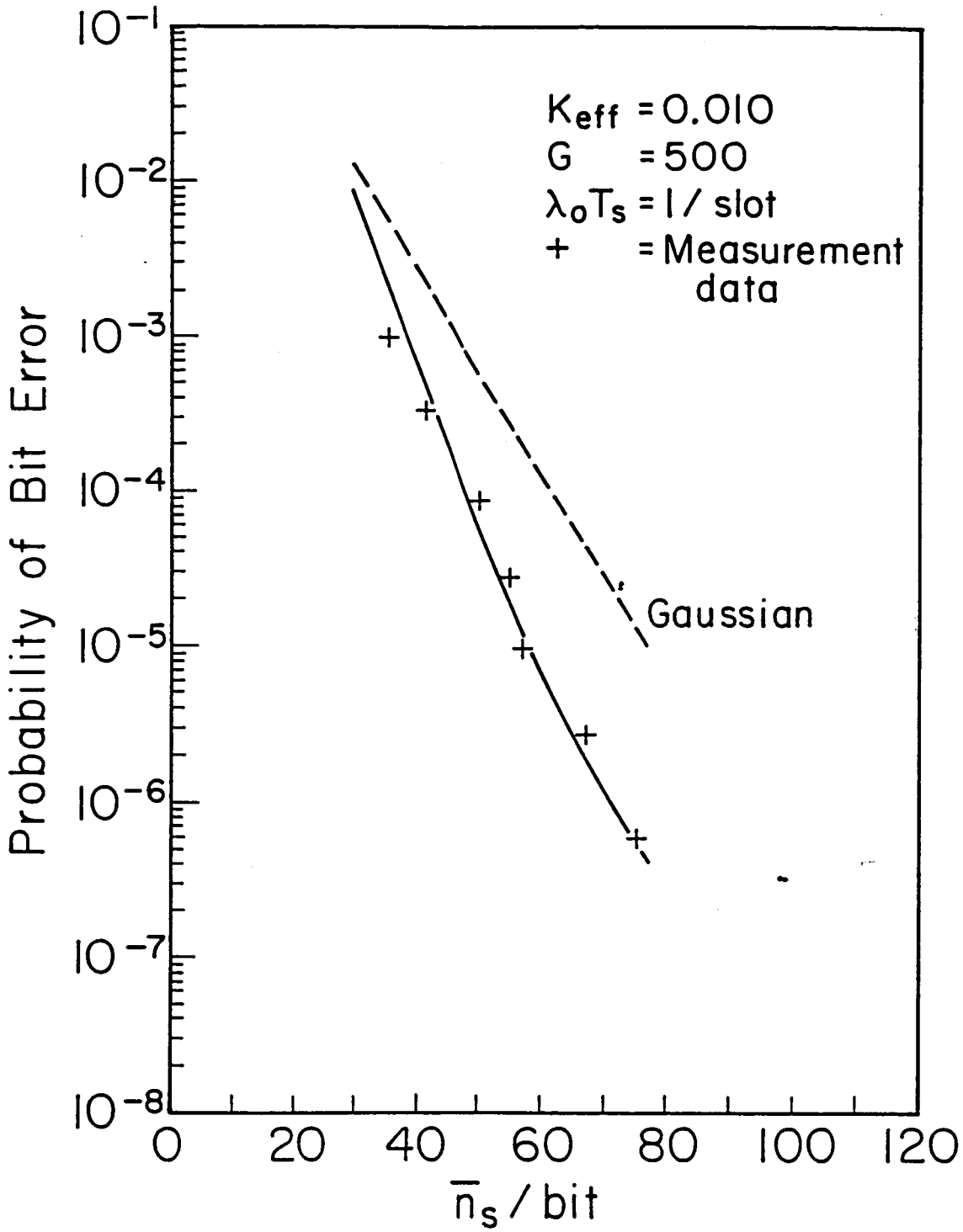
10^{-1}
10^{-2}
10^{-3}
10^{-4}
10^{-5}
10^{-6}
10^{-7}
10^{-8}
Probability of Bit Error
K_{eff} = 0.010
G = 500
$\lambda_o T_s$ = 1 / slot
+ = Measurement data
Gaussian
0
20
40
60
80
100
120
$\bar{n}_s$ / bit

Figure 6

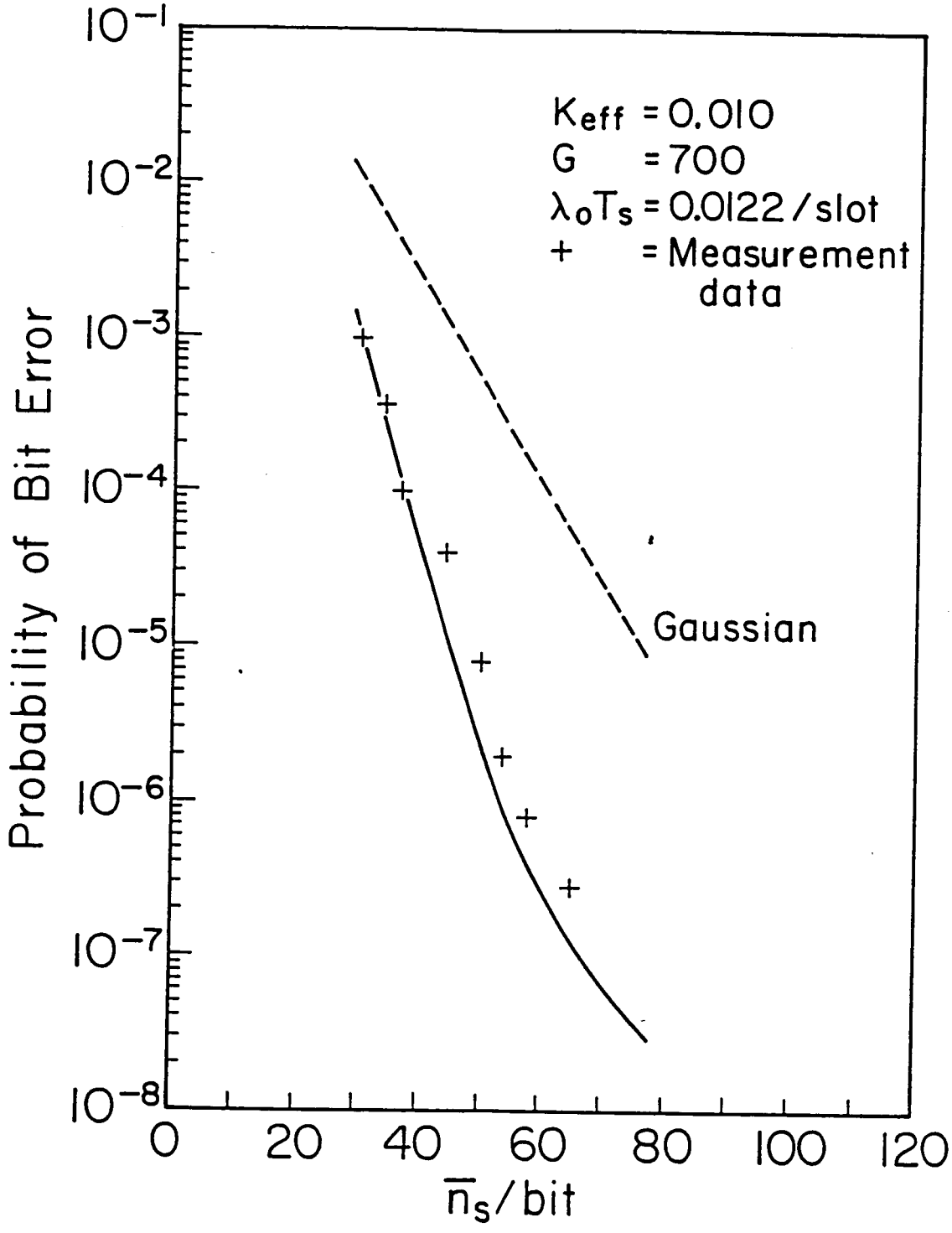
Probability of Bit Error
10^{-1}
10^{-2}
10^{-3}
10^{-4}
10^{-5}
10^{-6}
10^{-7}
10^{-8}
K_{eff} = 0.010
G = 700
$\lambda_o T_s$ = 0.0122 / slot
+ = Measurement data
Gaussian
0
20
40
60
80
100
120
$\bar{n}_s$ / bit

Figure 7